International Journal of Nanomedicine

Dovepress
open access to scientific and medical research

Open Access Full Text Article

ORIGINAL RESEARCH

Electrospraying Oxygen-Generating Microparticles for Tissue Engineering Applications

This article was published in the following Dove Press journal:
International Journal of Nanomedicine

Alan IS Morais[1,*]
Xichi Wang[2–4,*]
Ewerton G Vieira[1]
Bartolomeu C Viana[1,5]
Edson C Silva-Filho[1]
Josy A Osajima[1]
Samson Afewerki[3,4]
Marcus AF Corat[6]
Heurison S Silva[5]
Fernanda R Marciano[5]
Guillermo U Ruiz-Esparza[3,4]
Thiago D Stocco[6,7]
Mirian MM de Paula[6]
Anderson O Lobo[1]

[1]LIMAV-Interdisciplinary Laboratory for Advanced Materials, Materials Science and Engineering Graduate Program, UFPI-Federal University of Piauí, Teresina, PI CEP 64049-550, Brazil; [2]Department of Cardiovascular Surgery, Union Hospital, Tongji Medical College, Huazhong University of Science and Technology, Wuhan 430022, People's Republic of China; [3]Division of Engineering in Medicine, Department of Medicine, Harvard Medical School, Brigham & Women´s Hospital, Cambridge, MA 02139, USA; [4]Harvard-MIT Division of Health Science and Technology, Massachusetts Institute of Technology, MIT, Cambridge, MA 02139, USA; [5]Department of Physics, UFPI-Federal University of Piauí, Teresina, PI CEP 64049-550, Brazil; [6]Multidisciplinary Center for Biological Research, University of Campinas (UNICAMP), Campinas 13083-877, Brazil; [7]Faculty of Physiotherapy, Santo Amaro University, São Paulo 04829-300, Brazil

*These authors contributed equally to this work

Correspondence: Anderson O Lobo
Email lobo@ufpi.edu.br

Background: The facile preparation of oxygen-generating microparticles (M) consisting of Polycaprolactone (PCL), Pluronic F-127, and calcium peroxide (CPO) (PCL-F-CPO-M) fabricated through an electrospraying process is disclosed. The biological study confirmed the positive impact from the oxygen-generating microparticles on the cell growth with high viability. The presented technology could work as a prominent tool for various tissue engineering and biomedical applications.

Methods: The oxygen-generated microparticles fabricated through electrospraying processes were thoroughly characterization through various methods such as X-ray diffraction (XRD), Fourier Transform Infrared Spectroscopy (FTIR) analysis, and scanning electron microscopy (SEM)/SEM-Energy Dispersive Spectroscopy (EDS) analysis.

Results: The analyses confirmed the presence of the various components and the porous structure of the microparticles. Spherical shape with spongy characteristic microparticles were obtained with negative charge surface ($\zeta = -16.9$) and a size of 17.00 ± 0.34 μm. Furthermore, the biological study performed on rat chondrocytes demonstrated good cell viability and the positive impact of increasing the amount of CPO in the PCL-F-CPO-M.

Conclusion: This technological platform could work as an important tool for tissue engineering due to the ability of the microparticles to release oxygen in a sustained manner for up to 7 days with high cell viability.

Keywords: oxygen-generating-microparticles, electrospraying, tissue engineering, calcium peroxide, cartilage

Introduction

Cartilage is a connective tissue with a structurally organized extracellular matrix (ECM) composed of collagen and non-collagenous proteins, such as proteoglycans.[1] These cells are called chondrocytes and reside within gaps. Cartilage is generally devoid of blood vessels; thus chondrocytes exist in low oxygen tension and under limited nutrient conditions, so their cells must obtain their oxygen and nutrients by long-range diffusion of the perichondrium.[2] Chondrocytes are highly specialized cells and play a crucial role in maintaining the ECM, and their production is affected by the occupancy microenvironment.[2] Oxygen plays a key role in cell metabolism and viability, thus, oxygen supply is an important consideration during the culture of cartilage constructs for clinical applications.[3] Moreover, tissue hypoxia (deficiency in oxygen) often occurs after the destruction of the vascular tissue and this condition can result in cell death and necrosis.[4] The tensions of oxygen below 1% inhibit glucose uptake and lactate production, as well as cellular ribonucleic acid (RNA) synthesis.

Therefore, the presence of oxygen is a crucial factor for the chondrocytes that facilitates their basal metabolic activity.[5]

In addition, the use of oxygen-based materials has been investigated and developed in several areas,[6] such as radio therapy,[7] bone growth,[4] and regeneration of vascularized tissues.[8] These treatments may be an efficient method to block local hypoxia in the early stages of peripheral nerve injury.[9] Several reports have employed oxygenated polymeric microparticles (PMs) for in situ treatment involving cartilaginous tissue.[10] For instance, hybrid materials based on the combination of organic and inorganic components are new strategies for biomaterials with potential applications in the field of bioengineering. These oxygenated PMs can be considered intelligent biomaterials,[11] because oxygen delivery is triggered upon contact with water (H_2O), and their application allows both the structural defects of tissue reconstruction and recovery of the tissue functions lost due to damage.[12,13] Some of these inorganic biomaterials are used as oxygen generators and releasers at the application site, such as sodium percarbonate,[14,15] magnesium peroxide,[16] hydrogen peroxide (H_2O_2),[17,18] fluorinated compounds,[16] pyridine endoperoxides,[19] and calcium peroxide (CPO).[20] In 2015, Lee et al developed hollow microparticles (HPs) containing oxygen transporter as a structured system (scaffolds) that allowed the uniform distribution of oxygen to the adhered cells in the HPs.[21] In their results, tissue necrosis in a hypoxic environment was controlled. Moreover, McReynolds et al recently manufactured microspheres by encapsulating CPO in non-cytotoxic polydimethylsiloxane (PDMS). Structured microspheres (three-dimensional (3D) scaffolds) provided direct oxygenation to the affected areas and allowed the proliferation of β-pancreatic cells.[22] Additionally, oxygen-releasing microspheres were fabricated by combining H_2O_2, catalase enzyme, and a thermosensitive hydrogel. This system was able to release oxygen for about two weeks. In their results, a significant improvement in vascularization was observed with increased cardiosphere-derived cell survival (CDC) and cardiac differentiation under the hypoxia condition.[17]

Alginate coated poly(lactic-co-glycolic acid) (PLGA) microspheres with encapsulated H_2O_2 and their application to muscle cells under hypoxia condition have also been demonstrated.[18] The dual layered system (alginate and PLGA) allowed the controlled release of the oxygen at the optimal level for the survival of the muscle cells. Several approaches have been employed to design and fabricate polymer particles, such as solvent evaporation, emulsion diffusion, nanoprecipitation, microfluidic device, and electrospray. The difference lies primarily in the atomization techniques, the miscibility between the organic phase and the aqueous phase, or solvent removal techniques.[23] The presented work employs the electrospray approach due to its rapidness, ability to provide controlled manufacture of biodegradable spherical polymeric particles, and compatibility with peroxide-based materials. The electrospray technology has a single phase that combines solvent evaporation and fabrication. This provides a great advantage for certain types of peroxide materials compared to a microfluidic device and traditional emulsion methods. These approaches normally involve two or multiple phases and aqueous solutions, which may react with peroxide and result in extremely low efficacy. Moreover, the microfluidic device cannot be employed because the physical requirements of the organic phase and peroxide crystals cause a predicted high chance of blocking the system.[24] Moreover, other methodologies are slower and more complex, since, for the stabilization of the microparticles (M), large amounts of surfactant/cosurfactant are added, limiting both the solid polymer content and its application.[25]

Over the years, several polymers have been employed to fabricate microparticles such as Polycaprolactone (PCL), Poly (methyl methacrylate) (PMMA),[26] PLGA,[27] and Poly(vinylidene fluoride) (PVDF).[28] The Food and Drug Administration (FDA) approved PCL as abioresorbable polyester with high biocompatibility, which is biodegradable, non-toxic, and widely applied in the field of tissue regeneration.[13,29] Additionally, Pluronic F-127, is another clinically applicable polymer, with high biocompatibility and low toxicity,[30,31] which can be used as a hydrophilic additive when interacted with PCL.[31,32] Furthermore, the merging of F-127 with PCL improves the characteristics of PCL, such as enhanced surface wettability, and introduces surface porosity due to the interaction between the two components, which in turn improves the biological performance of the blend.[33]

Herein, we disclose for the first time the design and fabrication of porous surface microparticles (M) based on PCL, Pluronic F-127, and CPO through a facile electrospray technique. After the synthesis, the materials were characterized, and their ability to release oxygen molecules was investigated. Moreover, this biological study confirmed high cell viability against chondrocytes (Figure 1).

Methods and Materials

Materials

The following chemicals were purchased from Sigma Aldrich (St. Louis, MO, USA): Calcium peroxide (CPO,

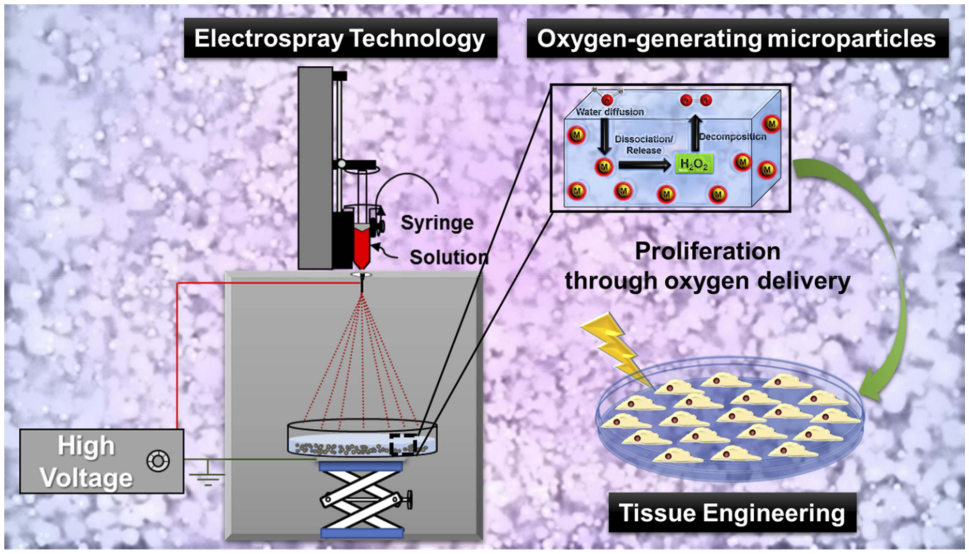

Figure 1 A schematic overview of the strategy to design and fabricate electrospray porous oxygen-generating microparticles (M) and their positive impact on the cell proliferation through sustained oxygen delivery.

CaO_2) powder with 200 mesh granulometry (CaO_2, analytical grade 75%), Dichloromethane (DCM, ACS reagent ≥99.5%), polycaprolactone (PCL, M_n = 45.000), PCL-80 (M_n = 80.000), Pluronic® F-127 (OE_{100} PO_{65} OE_{100}), and methanol (ACS reagent ≥99.5%). All these reagents were used without prior purification. In the syntheses, deionized H_2O (Milli-Q system) was employed.

Fabrication of the PCL-CPO Microparticles (PCL-CPO-M)

Initially, a PCL solution (100 mg/mL) in DCM was prepared and homogenized for 3 h and subsequently a CPO solution (50 mg/mL) in DCM was added. The reaction mixture was further stirred for 3.5 h. Afterward the reaction mixture underwent the same preparation, washing and drying procedure as described vide supra, providing the PCL-CPO-M.

Fabrication of the PCL-F127-CPO Microparticles (PCL-F-CPO-M)

A PCL solution (100 mg/mL) in DCM was prepared and homogenized for 3 h and further stirred for 2 h. Afterwards, the Pluronic F-127 (10 mg/mL) in DCM was added to the reaction mixture and further stirred for an additional 3 h. Next, the CPO solution (50 mg/mL) in DCM was added and stirred for 3.5 h. After washing and drying, the PCL-F-CPO-M were afforded.

The infusion rate for the electrospray technique was adjusted to 3.0 mL/h in the infusion pump, and the volume of the polymer solution in the syringe was 3.0 mL. The syringe used in this process was glass, and the needle was made of stainless steel and plastic (0.42 mm internal diameter and 1 inch). A voltage of 12 kV was applied. The positive phase was attached at the tip of the needle, and the ground attached to a stainless-steel metal plate covered with aluminum foil and located below a collector plate containing 100 mL of methanol solution. Next, the voltage was applied, and the initial solution of PCL was ejected into the spiral form (Taylor cone). Subsequently, upon the evaporation of the solvent, microparticles on the plate were collected.[70,71] After obtaining the microparticles by electrospray technique, the material was immersed in methanol and centrifuged (5000 rpm for 5 min) (Benchtop Centrifuge NI 1812 – NOVA INSTRUMENTS) in falcon tubes (50 mL), and the methanol was removed. The microparticles were then transferred to Eppendorf and centrifuged again (14,500 rpm for 15 seconds) (Bench Microcentrifuge NI 1801 – NOVA INSTRUMENTS). At the end of the process, the supernatant was removed, and deionized H_2O was added to wash the material. The washing process was repeated for about 10 replicates, ensuring complete removal of the methanol (the absence of methanol was confirmed by Fourier Transform Infrared Spectroscopy). For a better dispersion of the microparticles, they were exposed to a vortex agitation (AP-56 Solution Stirrer – Phoenix Luferco). Finally, the obtained PCL-F-CPO-M were stored under vacuum in a desiccator until completely dry.

Characterization

The samples were characterized by X-ray diffraction (XRD) techniques using a Shimadzu Labx-XRD 600 with Cu-Kα (λ = 15406 Å), 2θ in the range of 20° to 70°, with a scanning rate of 1°/min. The morphology analysis was performed by scanning electron microscopy (SEM), through a field emission electron source (SEM-EC) equipment with a field emission in-lens (FEI), model Quanta FEG-250. The samples were mounted on "stubs" using double-sided carbon tape and covered with gold. The working conditions in the SEM were, 8 to 20 KV, the working distance of 10 mm with spot 3. The working conditions for Energy Dispersive Spectroscopy (EDS) were 25 KV and spot 5 with a working distance of 10 mm. Fourier Transform Infrared Spectroscopy (FTIR) analyzes were done in powder using KBr pellets in transmittance in the region of 4000 to 400 cm^{-1} with 32 scans and 4 cm^{-1} resolution, Perkin Elmer-model equipment: spectrum 100. The thermogravimetric analysis (TGA) and its derivative (DTG) for each test were used between 5.00 and 7.00 mg, heated to 1000°C with a heating rate of 10°C/min in argon atmosphere, with a flow of 50.00 mL/min, alumina sample port, in the TA Instruments Q600 SDT equipment.

After fabrication of the MPs, they were immediately characterized for their polydispersity index (PDI) and average zeta-potential (ζ), using a Malvern Zetasizer Nano ZS instrument (Malvern Instruments Ltd, UK) (Model Nano-ZS90). For these measurements, samples were diluted in Milli-Q H_2O at a concentration of 1 mg/mL.

Contact angle (CA) values were recorded using a CCD camera to capture the images and computed using CAM2008 software (KSV Instruments®). For this, a layer of microparticles was electrosprayed directly on cover slips, and then, drops of 16 µL of ultrapure H_2O (resistivity better than 18.2 MΩ×cm) were used. Each drop was recorded 20 times, and the average angle was computed. The CA values were obtained using the mathematical adjustment from Young/Laplace fitting.

Oxygen Release Study

The Oxygen release kinetics from the PCL-F-CPO-M with various concentrations of the CPO (0.5, 1, and 2%) were investigated by using needle-type microsensors (PreSens oxy-4, Regensburg, Germany) in a standard cell culture incubator under hypoxic conditions. First, the system was calibrated by setting the 0% point by measuring the O_2 level of a 1% (w/v) sodium sulfite aqueous solution, and the 100% point was set by measuring H_2O, which was oxygenated before by bubbling through air for 30 min. The dissolved oxygen (DO) was measured by placing three individual samples of the PCL-F-CPO-M in a 12-well plate loaded with 3 mL phosphate buffer solution containing catalase (100 U/mL) in each well and then placed in a 1% O_2 incubator. The pH was monitored during the whole process (which remained at ~7.4).

In vitro Cell Culture

The study was conducted in full accordance with the Guiding Principles for the Care and Use of Laboratory Animals approved by the Animal Care Committee guidelines at the Federal University of São Paulo (protocol no. 2478130315).

Chondrocytes Isolation and Expansion

Primary chondrocytes were harvested from articular cartilage of the knee joints of Wistar rats (130–150 g). Briefly, articular cartilage layers of the knee joints were sliced and minced and digested in 0.25% type I collagenase (Sigma-Aldrich, USA) in Dulbecco's modified Eagle's medium (DMEM; Gibco-Invitrogen, USA) at 37°C in a 5% CO_2 incubator overnight. After that, cells were collected from the digestion solution and seeded onto tissue culture flasks, for expansion in monolayer, and kept as sub-confluent monolayers in growth medium, DMEM supplemented with 1.5 mL glutamine, 10% fetal bovine serum (FBS), and 100 units/mL penicillin–streptomycin (Gibco-Invitrogen, USA). The cells were expanded using standard tissue culture techniques, in which the incubations occurred in a 5% CO_2 atmosphere at 37°C and culture medium was changed every 3 days. After 80% confluence, the cells were trypsinized and replaced at the same density until the third passage (P3). The P3 chondrocytes were used in the following experiments. The chondrocytes phenotypes were tested by quantitative real-time PCR for gene expression of collagen type 1 (Col1) and type 2 (Col2) and Sox9, which were all compared with internal control GAPDH (Supplementary File).

Cell Encapsulation and 3D Culture

To evaluate the cell viability, chondrocytes were encapsulated in the Gelatin Methacryloyl (GelMA, Sigma-Aldrich, USA) hydrogel containing different concentrations of PCL-F-CPO-M microparticles: 0% (control), 0.5%, 1%, and 2% w/v. Briefly, chondrocytes were trypsinized, collected by centrifugation, counted with a hemocytometer,

and re-suspended in the DMEM solution containing GelMA (10% w/v) and photoinitiator (0.5% w/v) [(2-hydroxy-4′-(2-hydroxyethoxy)-2-methylpropiophenone; Irgacure 2959; Sigma-Aldrich, USA] at a final cell density of 6×10^6 cells/mL. Then, the different concentrations of PCL-F-CPO-M were added. The four different final solutions were pipetted into 96 well plate and cured with UV light (wavelength: 360–480 nm; 6.9 mW/cm^2; Omnicure Series 2000, EXFO, Canada) for 5 min for gel formation with 2.5 mm thickness. Culture medium, composed of DMEM supplemented with 1.5 mL glutamine, 10% fetal bovine serum (FBS), and 100 units/mL penicillin–streptomycin was added immediately after gel formation. The cell-laden hydrogels were maintained at 5% CO_2 atmosphere at 37°C, and the culture medium was changed every 3 days.

Cell Viability Assay

Cell viability in the cell-laden hydrogels with different PCL-F-CPO-M concentrations was determined on days 1 and 5, after using Hoechst 33,342 (Thermo Fisher Scientific, USA) and Propidium Iodide (Thermo Fisher Scientific, USA) to stain the cells. Briefly, the cell-laden hydrogels were washed with Phosphate Buffered Saline (PBS) and incubated in Culture medium with a concentration of 0.2 μg.mL^{-1} Hoechst 33,342 and 0.2 μg.mL^{-1} PI for 30 min at 37°C. Subsequently, the hydrogels were rinsed again in PBS, and stained cells were viewed using an ImageXpress Micro® Confocal High-Content Imaging System (Molecular Devices, USA). The images were captured with a 10× objective (9 images per well) and analyzed by the Multi-Wavelength Cell Scoring Application module for MetaXpress® Software (Molecular Devices, USA). Cell viability was based on the percentage of live cells, determined by the method of exclusion of the dead cells (red fluorescence) from the total amount of cells (blue fluorescence).

Statistical Analysis

All data were reported as the mean ± standard deviation (SD) of three independent samples of each PCL-F-CPO-M concentration (triplicate wells). Statistically significant differences between groups of samples were evaluated by one-way ANOVA followed by Tukey's post hoc analysis, and p-values <0.05 were considered statistically significant. All statistical analyses were executed using Minitab version 17 software (Minitab Inc., USA).

Results and Discussion

The microparticles were prepared by the electrospray technique.[34] An overview of the synthetic strategy is demonstrated in Figure 2, along with the various components and their respective masses and concentrations employed in the design of the microparticles. Three different microparticles (M) were prepared: first, microparticles based on solely PCL (PCL-M); second, a combination of PCL and CPO (PCL-CPO-M); and finally, PCL, F-127, and CPO (PCL-F-CPO-M). They were all prepared following the same procedure, as described in the experimental section. Briefly, a PCL solution (100 mg/mL) was prepared and homogenized for 3 h and further stirred for 2 h. Afterwards, the Pluronic F-127 (10 mg/mL) was added to the reaction mixture and further stirred for an additional 3 h. Next, the CPO solution (50 mg/mL) was added and stirred for 3.5 h. Subsequently, the mixture solution underwent the electrospray technique, followed by evaporating the solvent to provide the microparticles. Next, the microparticles underwent several washing steps, and after drying the PCL-F-CPO-M were produced.

The various fabricated microparticles were thoroughly characterized. The X-ray diffraction (XRD) analysis of the microparticles (PCL-M, PCL-CPO-M, and PCL-F-CPO-M) are presented in Figure 3A. The typical reflections of the PCL were identified with two intense peaks at 21.30° and 23.60°, which are characteristic of the semi-crystalline nature of PCL (Figure 3A-i).[29,35] Moreover, the main characteristic peaks of the CPO are located at 30.20°, 35.58°, 47.31°, attributed to CaO_2 according to the JCPDS code 01-085-0514 (Figure 3A-ii and iv).[36] The peaks attributed to the calcium carbonate ($CaCO_3$) (card No. 01-072-0506 and 01-083-0578) and $Ca(OH)_2$ (card No. 00-044-1481) are also found in the diffractogram.[37] Furthermore, the PCL reflections were identified in the XRD of the PCL-CPO-M and PCL-F-CPO-M, and the CPO-related peaks were also observed with adequate clarity and intensity (Figure 3A-iii and iv). These peaks are consistent with those presented in the literature, which confirms that the CPO was successfully incorporated in our microparticles. Moreover, after interaction between the materials, the characteristic reflections of PCL were maintained, and the presence of intermediate phases was not observed.[38]

Additionally, the materials were characterized by Fourier Transform Infrared Spectroscopy (FTIR) analysis (Figure 3B). The CPO showed the absorption band at 3000 to 3700 cm^{-1},

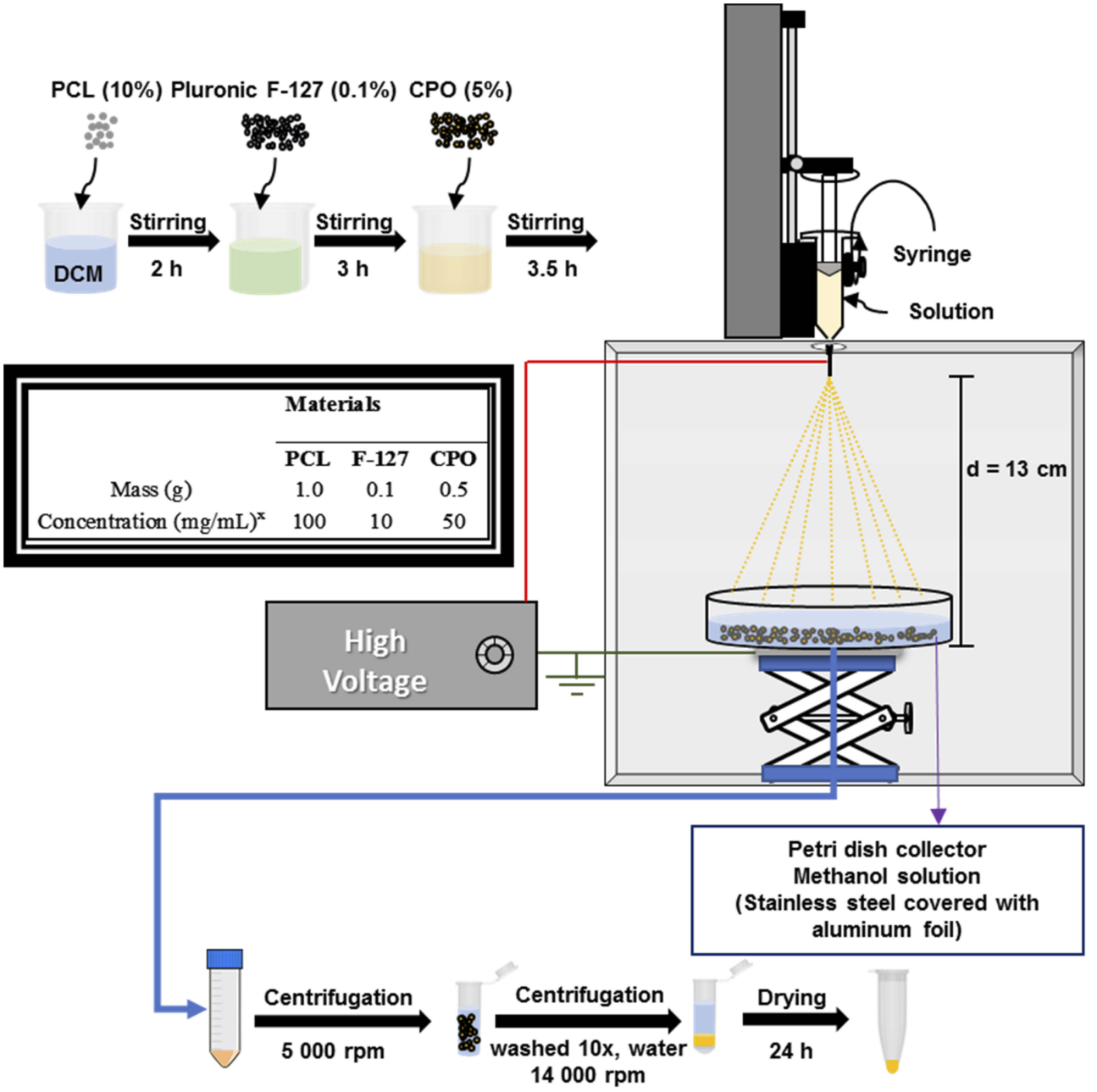

Figure 2 A schematic overview of the fabrication strategy for the electrospray technique in the design and preparation of the PCL-M, PCL-CPO-M, and PCL-F-CPO-M and a table showing the masses and concentration employed for the different materials for the preparation of the presolutions. [x]The solvent used for the preparation of the solutions was dichloromethane (DCM).

which is attributed to the elongation mode of the -OH group of the CPO converted to H_2O molecules and in the 1635 cm^{-1} band referring to the HOH deformation of residual-free H_2O (Figure 3B-i). Peaks corresponding to the O-Ca-O bending vibration mode of CaO_2 and CO_3^2 of the calcite group could be observed in the wide range of 1600 to 1300 cm^{-1}, thus corroborating with the XRD results of the materials with CPO (Figure 3A-ii, iii and iv).[37] The absorption band at 875 cm^{-1} is attributed to the oxygen (O-O) bridge of CPO.[39] All the important peaks of the PCL such as the 2945 cm^{-1} correspond to bands associated to the vibrations of asymmetric elongation $\upsilon_{as}(CH_2)$; symmetrical stretch $\upsilon_s(CH_2)$ at 2865 cm^{-1}; carbonyl elongation at 1725 cm^{-1} υ(C=O), 1473, 1397, and 1361 cm^{-1} (CH_2) bending; elongation in the crystalline phase at 1295 cm^{-1} υ_{cr}(C-O; C-C); asymmetrical stretching υ_{as}(C-O-C) at 1241 cm^{-1}; and stretching vibration ν(OC-O) at 1188 cm^{-1} were also identified (Figure 3B-ii).[40–43] Moreover, the characteristic bands of PCL were also observed

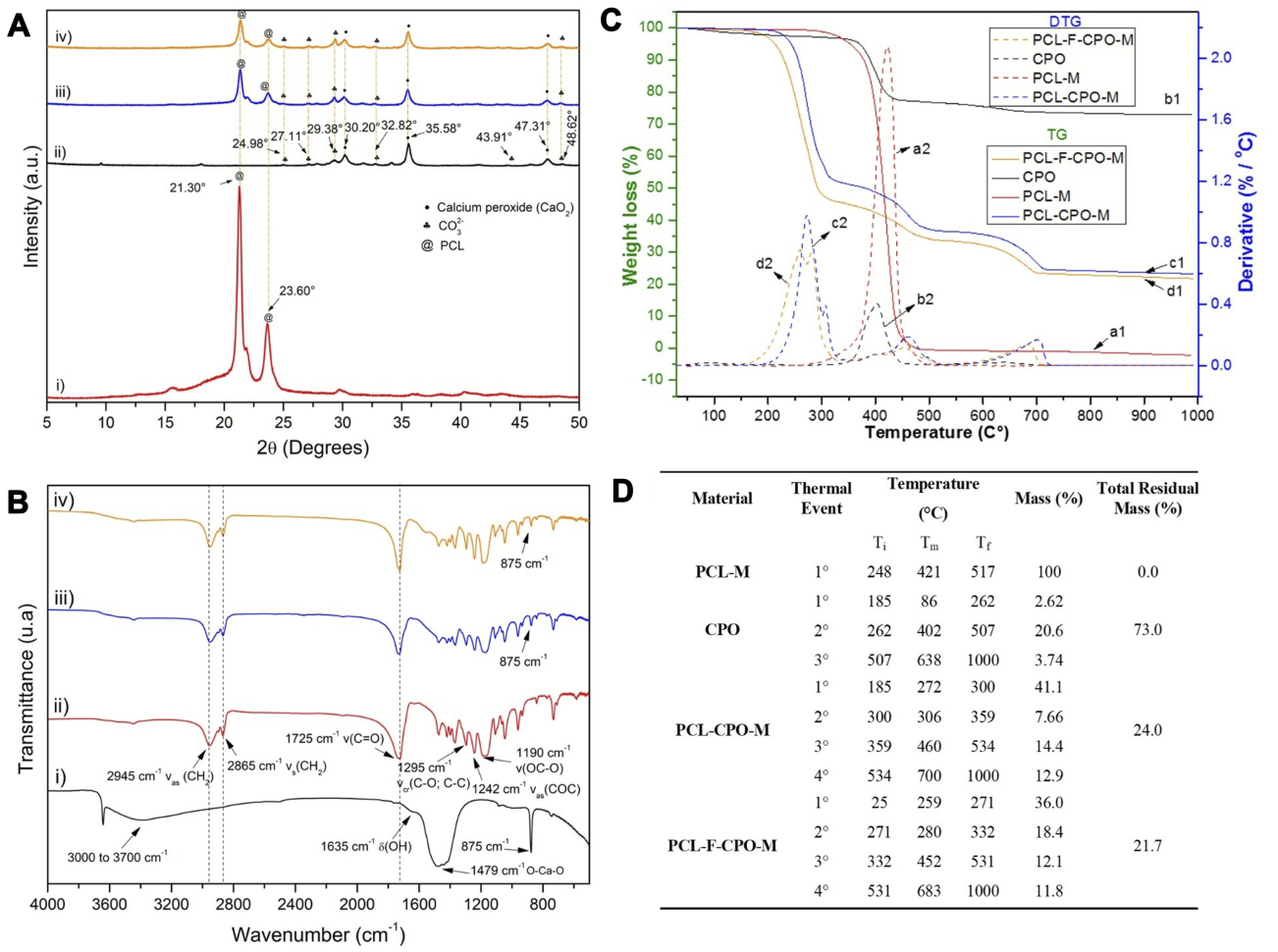

D

Material	Thermal Event	Temperature (°C)			Mass (%)	Total Residual Mass (%)
		T_i	T_m	T_f		
PCL-M	1°	248	421	517	100	0.0
CPO	1°	185	86	262	2.62	73.0
	2°	262	402	507	20.6	
	3°	507	638	1000	3.74	
PCL-CPO-M	1°	185	272	300	41.1	24.0
	2°	300	306	359	7.66	
	3°	359	460	534	14.4	
	4°	534	700	1000	12.9	
PCL-F-CPO-M	1°	25	259	271	36.0	21.7
	2°	271	280	332	18.4	
	3°	332	452	531	12.1	
	4°	531	683	1000	11.8	

Figure 3 Characterization of the various samples. (**A**) The X-ray diffraction (XRD) of the i) PCL-M, ii) CPO, iii) PCL-CPO-M, and iv) PCL-F-CPO-M. (**B**) Fourier Transform Infrared Spectroscopy (FTIR) of the i) CPO, ii) PCL-M, iii) PCL-CPO-M, and iv) PCL-F-CPO-M. (**C**) Thermogravimetric analysis (TG) and its derivate (DTG) of the i) PCL-M, ii) CPO, iii) PCL-CPO-M, and iv) PCL-F-CPO-M. (**D**) Table presenting the event relationship between the DTG of CPO and the microparticles PCL-M, PCL-CPO-M, and PCL-F-CPO-M. Definitions; T_i = Initial temperature, T_m = Maximum temperature, and T_f = Final temperature.

in the PCL-CPO-M and PCL-F-CPO-M spectra as well as the presence of the CPO by the appearance of the band at 875 cm $^{-1}$ (Figure 3B-iii-iv). The absence of the 1479 and 3700 cm^{-1} bands of CPO can be attributed to the interactions of the oxygen in the OH and CaO_2 with the polymers. All bands characteristic of PCL are observed in each microparticle; however, in the PCL-F-CPO-M, which contains Pluronic F-127 in its composition, the vibrations of $\upsilon_{as}(CH_2)$, $\upsilon_s(CH_2)$ and υ(C=O) cannot be identified, probably due to the overlapping with the PCL bands.

Furthermore, the thermogravimetric analysis (TG) and its derivative (DTG) analysis for all the materials prepared are presented in Figure 3C. The PCL-M showed a single event with maximum degradation temperature (T_{max}) at 421°C (Figure 3C.a2), with total degradation of organic chain at 476°C (Figure 3C.a1).[44,45] This single event indicates the decomposition of the PCL that undergoes chain scission through the random pyrolysis of the ester groups, releasing carbon dioxide (CO_2), H_2O, and hexanoic acid, followed by the formation of the ε-caprolactone (cyclic monomer), resulting from a depolymerization process of decompaction.[46,47] The TG curve for the CPO in Figure 3C.b1 shows typical losses of the CPO with three events presented in Figure 3C. b2 and D. The first event up to 100°C is related to H_2O loss and the second event denotes oxygen release (402°C). The third event[48] may be related to loss of oxidation of oxygen or the decomposition of $CaCO_3$ calcite with its decomposition from 500°C to 700°C, corroborating with the XRD and FTIR spectra in Figure 3A and B.[39,49] Moreover, the TG curve for the PCL-CPO-M indicates a change in the mass of the material and is attributed to the insertion of the CPO into the PCL-M (Figure 3C.c1). Four events can be observed, in which the first (184°C) can be attributed to mass loss of physisorbed H_2O that may be on the surface of the

microparticles, and concomitantly, the first and second loss of mass (300°C) events are related to the PCL that underwent modification due to the CPO (Figure 3C.c2). Previous studies demonstrated with the oxides inserted into the PCL interfere in the polymer chain, indicating a discontinuity of the monomers, as can be seen in the XRD (Figure 3A-iii), in which the material becomes less crystalline than the PCL-M.[50] Another factor that may have occurred is the interference of the two steps of chain scission by means of random pyrolysis of the ester groups and the formation of ε-caprolactone that occur in PCL, thus causing the appearance of these two first events. Furthermore, the third event (358°C) may be correlated with the loss of oxygen from the CPO.[48] In addition, the fourth event (533°C) may be related to the decomposition of calcite.[39] The same phenomena that proceeded with the PCL-CPO-M could also be observed in the PCL-F-CPO-M but with a slight decrease in mass loss temperature, as depicted in Figure 3C.d1, and the decrease in melting point due to the presence of the Pluronic F-127 in the material, evident in the small increase of percentage of mass loss. This difference can be attributed to the presence of Pluronic F-127, in the polymer degradation region, in which there is only one wide event, and the other at a slightly higher temperature, which must be from the disintegration of the Pluronic F-127, probably because the polymer is more external and degrade first.

The morphology of the various microparticles fabricated was investigated using scanning electron microscopy (SEM) and SEM-Energy dispersive X-ray spectroscopy (EDS) analysis (Figure 4A–F). The PCL-M (Figure 4A) microparticles were mostly round and ranged from 18 to 28 μm, with an average size of 23.00 ± 0.46 μm in diameter (Figure 4G). SEM revealed that these microparticles were dispersed, unlike the CPO particles, which may increase the surface area of the microparticles. Moreover, the EDS mapping confirmed that the PCL-M does not contain any CPO (Figure 4D). The PCL-CPO-M displayed mostly oval morphology, although some round particles were also observed and microstructures with rectangular and slightly spongy morphology appeared on its surface (Figure 4B). The EDS mapping revealed the presence of calcium (Ca) in the PCL-CPO-M, indicating that a CPO layer covered the oval or round PCL-M microparticles (Figure 4E). These results corroborate the results of XDR (Figure 3A-iii) and the FTIR (Figure 3B-iii). The size of the PCL-CPO-M increased compared to the PCL-M to particle size of 46.00 ± 0.75 μm in diameter (~factor 2) (Figure 4H). The surface morphology of the microparticles clearly changed after the addition of the Pluronic F-127 (PCL-F-CPO-M) (Figure 4C). The microparticles maintained their spherical shape; however, the surface displayed a spongier characteristic. The presence of the Pluronic F-127 favored a decrease in the size of the microparticles, for an average of 17.00 ± 0.34 μm (Figure 4I). The EDS mapping of the PCL-F-CPO-M also confirmed the presence of CPO in the microparticles (Figure 4F).

In addition, the charge and zeta potential (ζ) distribution of the microparticles and the CPO are presented in Figure 4J. The negative ζ of the PCL-M (ζ = –31.5) are consistent with previously reported data.[51,52] On the other hand, the CPO displayed positive charge (ζ = 5.12); thus, the ζ of the PCL-CPO-M showed a decrease of negative charge (ζ = –15.3) compared to the PCL-M. Furthermore, the addition of the Pluronic F-127 (PCL-F-CPO-M) did not have a significant impact on the zeta potential (ζ = –16.9), only slightly increasing the negative charge.

The obtained results can be compared to previously report performed on PCL and Pluronic F-127 combination, where the appearance of pores on the surface was observed due to the presence of the Pluronic F-127, which also resulted in the increase of the hydrophilicity of the PCL (Figure 4K)[32,53–55] To probe the changes in hydrophobicity, the CA was measured by forming a film of PCL-M, PCL-CPO-M, and PCL-CPO-F-M deposited by electrospray on glass substrate. Each CA value represents an average of 20 measurements. The PCL-M and PCL-CPO-M presented high hydrophobicity, due to the PCL composed of hydrophobic aliphatic chains.

For the PCL-CPO the increase of CA is probably due to the adsorption of Ca^{+} ions on the PCL especially near (negative sites) the oxygen atoms, reducing the charge density, thus shielding the hydrogen bond instead of increasing the hydrophobic interaction. Interestingly, the drop onto the PCL-CPO-F-M film did not provide any CA because the drop was completely absorbed by the film (Figure 4K). This was expected to ensue due to the structure of F-127, comprised of hydrophobic and hydrophilic parts with the ratio 1:2. According to Wang et al, such hydrophilic tails are oriented out of the surfaces of the microparticles, exposing a highly hydrophilic layer.[56]

Additionally, the oxygen release assay (ORA) of the PCL-F-CPO-M at different concentrations of CPO (0.5%, 1%, and 2% w/v) was investigated and is depicted in Figure 5A. The mean oxygen release decays (C_{OR}) for the PCL-F-CPO-M formulations (0.5%, 1%, and 2% w/v) were calculated by the mean $\Delta_{oxygen\ release}$, which was

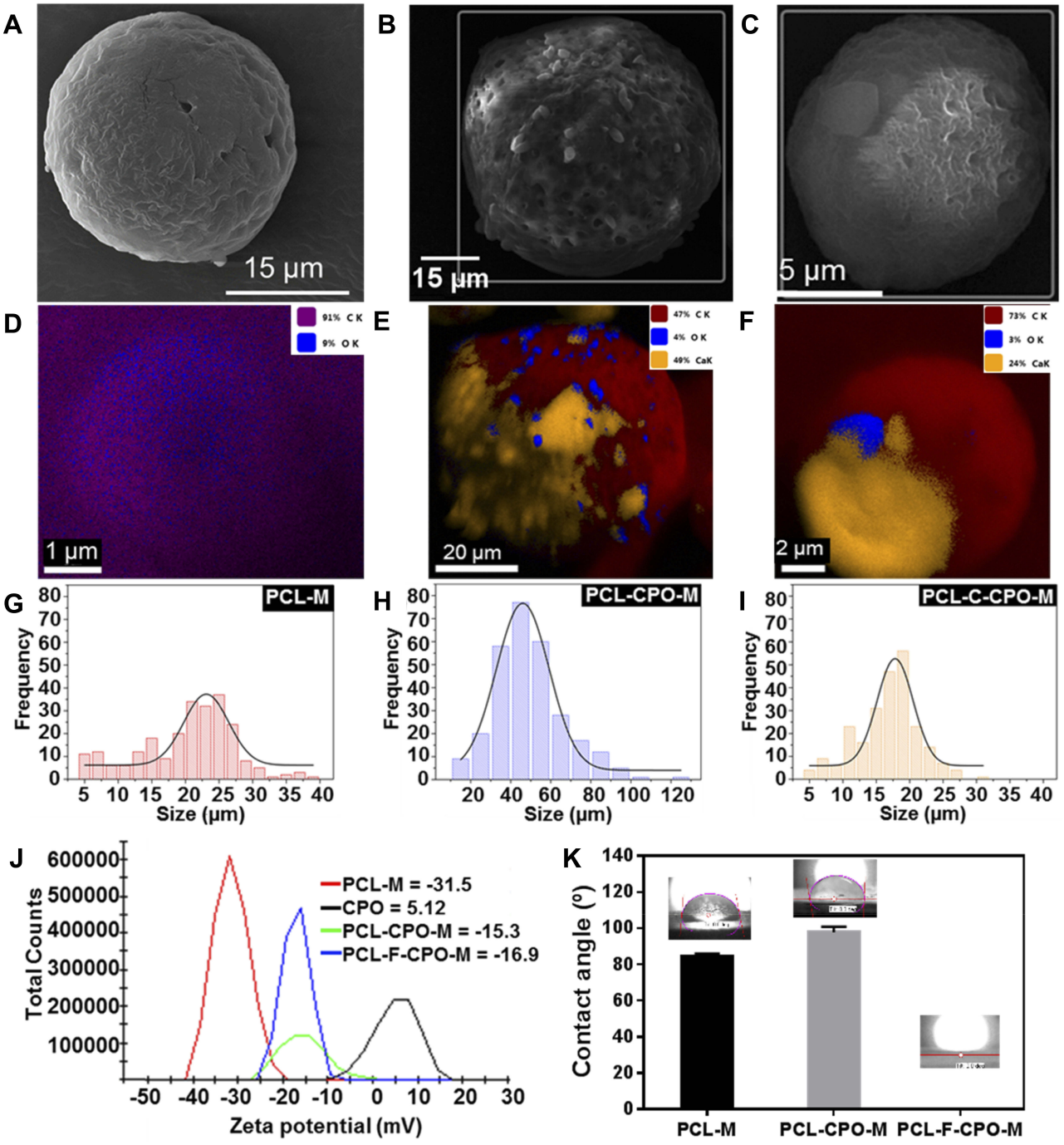

Figure 4 Scanning electron microscopy (SEM) image of the various microparticles (**A**) PCL-M, (**B**) PCL-CPO-M, and (**C**) PCL-F-CPO-M. The SEM-Energy dispersive X-ray spectroscopy (EDS) of the (**D**) PCL-M, (**E**) PCL-CPO-M, (**F**) PCL-F-CPO-M. The size distribution presented in the histogram of the (**G**) PCL-M, (**H**) PCL-CPO-M, and the (**I**) PCL-F-CPO-M. (**J**) The zeta potential distribution of the fabricated microparticles and the CPO. (**K**) Contact angle (CA) of the films deposited by electrospray on glass substrate.

calculated from day 1 (C_1) to 6 (C_6), with the assumption that gas transport occurred via pores. For day 7 (C_{day7}), the released concentrations of oxygen were gradually decreased until the lack of oxygen production (Figure 5A). The values reported in Figure 5A for the C_{OR} are calculated following Equation 1.

$$C_{OR} = \frac{(C_2 - C_1) + (C_3 - C_2) + (C_4 - C_3) + (C_5 - C_4) + (C_6 - C_5)}{5} \quad (1)$$

The release profile showed that the microparticles provided an initial oxygen release on the first day (C_1) of 10.1 ± 1.8, 10.5 ± 0.8, and 10.3 ± 1.2 mg/mL, for the

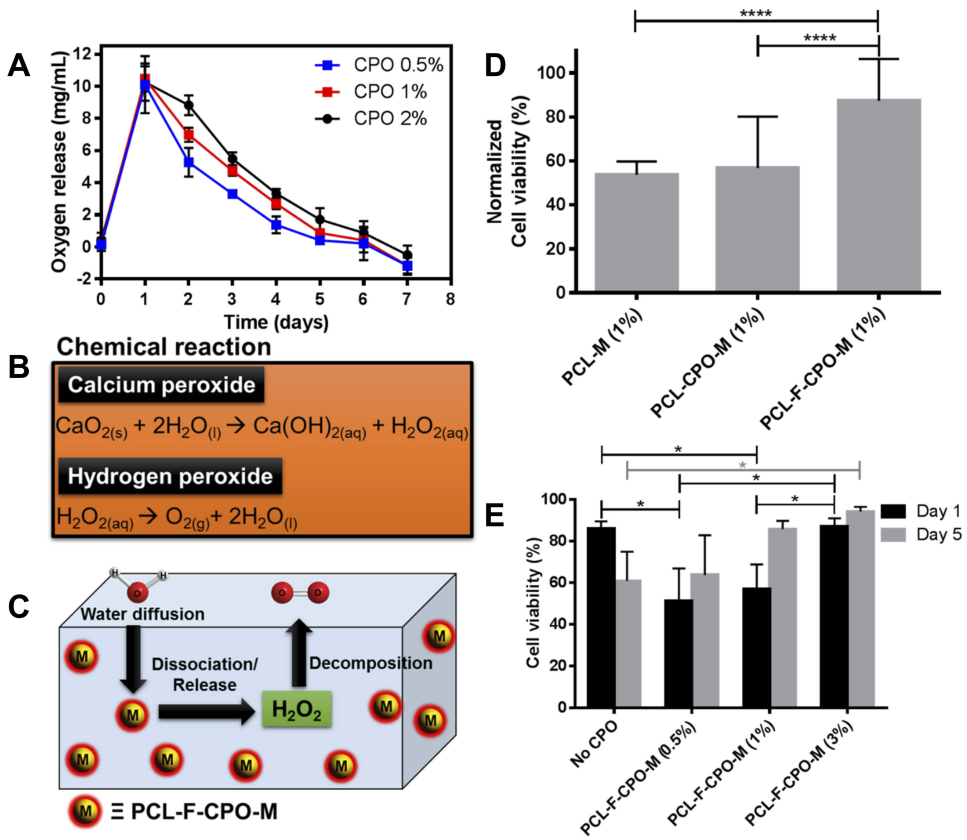

Figure 5 (**A**) The oxygen release assay with three different concentrations of the CPO in the PCL-F-CPO-M for up to 7 days. (**B**) The chemical reaction for the release/dissociation of the CPO into free oxygen in the presence of water (H_2O). (**C**) A schematic image describing the process to release oxygen from our microparticle system (PCL-F-CPO-M). (**D**) The cell viability results from rat chondrocytes encapsulated in 10% GelMA hydrogel with the various microparticles (PCL-M (1%), PCL-CPO-M (1%) and PCL-F-CPO-M (1%)). The data are normalized between 1 and 5 days in 3D cell culture (n = 3). (**E**) The cell viability results from rat chondrocytes encapsulated in 10% GelMA hydrogel with varying concentrations of PCL-F-CPO-M (2%) after 1 and 5 days in 3D cell culture (n = 3). Data are expressed as mean ± standard deviation, N = 3. ANOVA ($p< 0.05$) following by Tukey's multiple comparison tests. *$p< 0.05$, ****$p< 0.001$.

systems with 0.5%, 1%, and 2% w/v of CPO, respectively. On the first day, the amount of oxygen released remained similar despite the different loading of the CPO (0.5%, 1%, and 2% w/v). However, on day 2 (C_2), the amount released from the different systems (0.5%, 1%, and 2% w/v) differed slightly with 5.3, 7.0, and 8.8 mg/mL oxygen release, respectively. The calculated kinetics of the released oxygen (C_{OR}) from the three formulations (0.5%, 1%, and 2%) of the PCL-F-CPO-M were 2.6, 2.0, and 1.8 mg/mL/day, respectively. These results indicated that higher concentration of CPO in the system provided a more sustained and slower release.

Biological studies were performed, on rat chondrocytes encapsulated in GelMA hydrogels with the various microparticles (PCL-M (1%), PCL-CPO-M (1%), and PCL-F-CPO-M (1%)). For this purpose, fluorescent microscopy images of stained cells (blue fluorescence for total cells and red fluorescence for dead cells) were used to investigate cell viability. The cell viability displayed significant difference when the microparticles contained the CPO, and the PCL-F-CPO-M (1%) group obtained the highest performance (Figure 5D). Based on these results, we performed further tests on the groups containing four different concentrations of PCL-F-CPO-M and cultured for 1 and 5 days. In contrast to the results observed with hydrogel containing only GelMA, the cell-laden hydrogels with PCL-F-CPO-M demonstrated a significant increase in the percentage of live cells from 1 to 5 days ($p<0,05$) (Figure 5E). Furthermore, the positive impact of increasing the amount of CPO in the PCL-F-CPO-M could be observed in the increased cell viability (significant difference occurred on Day 1 and for the group without any CPO on Day 5). This could be related to the increase of oxygen supply to the cells provided by the CPO.

Although, in articular cartilage, chondrocytes adapt to a low oxygen level environment (oxygen tension is about 7%), at least some oxygen is essential for their basal metabolic activity.[5,57,58] Chondrocytes have mitochondria,

and oxygen levels below 1% inhibit lactate production, glucose uptake, and cellular ribonucleic acid (RNA) synthesis.[59] Moreover, in osteoarthritis (OA), the main source of energy metabolism is altered from oxidative phosphorylation to glycolysis, caused by microenvironmental alterations, including hypoxia, evidencing the role of oxygen in chondrocytes metabolism in healthy joints and in the treatment of cartilage degeneration.[59] In accordance with previous studies,[17,21,60–62] these results demonstrated that incorporating oxygen-generating particles within the hydrogel scaffolds could facilitate cell survival for a longer period of time. Thus, the cells may synthesize extracellular matrix, while the scaffolds are gradually being degraded and reabsorbed, ultimately forming new cartilage tissue. However, to provide a continued supply of oxygen to cells within hydrogels, oxygen must be gradually released over time, and therefore, longer cell culture studies should be performed.

This study provided an important fundamental understanding and information for the future employment of microspheres as in situ oxygen generators to prevent cell death. The addition of CPO within the microparticles resulted in a significant increase of oxygen in the solution. Solid inorganic peroxides, such as CPO, are known biomaterials that generate oxygen in aqueous solutions and, consequently, similar mechanism occurs in the physiological fluids of the body.[16] The chemical reaction upon H_2O contact with CPO is depicted in Figure 5B, where in the first step the CPO is converted to H_2O_2 and subsequently, the H_2O_2 is transformed to free oxygen (O_2) and H_2O. A schematic process for the release of O_2 from our designed microparticles (PCL-F-CPO-M) is presented in Figure 5C. This demonstrates the ability of the microparticles to decompose upon contact with physiological solution and thereby generate oxygen within the implanted region. However, intermediate products formed from the oxygen-releasing components (eg, H_2O_2) can sometimes result in undesirable cytotoxicity, when present in high concentration.[6] Nevertheless, the cells have a defense mechanism in the ability to convert these intermediates into non-toxic products (eg, H_2O and O_2, Figure 5B and C).[4] In this context, the average physiological concentrations of oxygen in humans are about 4–7% and in some pathological ischemic tissues can drop to 1% (hypoxia).[63] Therefore, a sustained release of the CPO from the PCL-F-CPO-M based on the ORA could provide an optimal physiological condition, thus promoting a high rate of cell viability and, in the case of biomaterial implant, promote formation of blood vessels at the implanted site. Pathologies and their treatment can lead to tissue damage caused by trauma, inflammation, or ischemic diseases, further leading to local conditions of hypoxia and catabolism due to the lack of vascularization. Lv et al reported that films containing CPO (20 w/w%) presented an excellent cell response in vitro for proliferation.[64] The oxygen solubility will be proportional to the partial pressure (Henry's law); therefore, oxygen-generating biomaterials store an adequate amount of oxygen due to the van der Waals interaction between the oxygen and the surface of the materials. Thus, the release of oxygen will not only occur in the implanted areas, but the complete oxygenation in the microenvironments will positively affect and support the growth of cells in the neighboring tissues that may be found in a hypoxia environment.[6,21] Shiekh et al developed oxygen-releasing antioxidant polymeric cryogel scaffold containing CPO, which presented an oxygen release for about 10 days, and the in vivo study using an ischemic flap model demonstrated the prevention of tissue necrosis up to 9 days.[65] The in vitro cellular cytotoxicity assay, under hypoxic conditions, revealed that peroxide containing materials provided superior cell viability than the control (CPO without coating). Particularly in the initial stage of healing, hypoxia signaling is highly relevant. For example, after tissue injury reactions are induced at the cellular biological level, activated platelets lead to the migration of mesenchymal progenitor cells, and endothelial cells into a hypoxic environment that can modulate the cellular response.[66,67] Thus, the rate of oxygen release significantly impacts the formation of new tissues. Here, it is believed that the oxygen supply in the treated regions is largely dependent on vascularization and blood oxygenation on site, while the demand for oxygen is largely determined by the rate of cellular respiration.[4,68]

Very recently, Shen et al disclosed the preparation of oxygen-releasing PCL-CPO composite microspheres through electrospraying approach.[69] However, in our proposed technology, we engineered PCL-F-CPO-M with improved properties. The importance of having the Pluronic F-127 incorporated in the composite can be observed in our experimental data, such as improved hydrophilicity (the PCL-F-CPO-M presented a superhydrophilic nature with contact angle (CA) = 0°, while the PCL-CPO-M displayed high hydrophilicity that provide CA = 97.7°), smaller sized microparticles could be engineered compared to the PCL-CPO-M (PCL-F-CPO-M = 17.00 ± 0.34 μm and PCL-CPO-M = 46.00 ± 0.75 μm in diameter). Moreover, a significant improvement in the cell viability was obtained with our engineered particles (PCL-F-CPO-M) compared to the PCL-CPO-M. In this study, we

demonstrate the design and employment of the PCL-F-CPO-M as a good candidate for oxygen-generating biomaterial with the potential to promote blood vessel and cell growth, even under hypoxia microenvironments.

Conclusion

Porous surface microparticles made of PCL, Pluronic F-127, and CPO were prepared through a facile electrospray technique. The thorough characterization performed through XRD, FTIR, TG/DTG, and SEM/SEM-EDS confirmed the structure and composition of the fabricated microparticles. The XRD presented the characteristic peaks of the CPO thus corroborating the results of the FTIR, TG/DTG, and SEM/SEM-EDS. Furthermore, the SEM analysis revealed that the fabricated microparticles displayed a spherical shape with negative charge ($\zeta = -16.9$) and a size of 17.00 ± 0.34 μm. The disclosed technological platform could work as an important tool for tissue engineering application, particularly due to the ability of the microparticles to release oxygen in a sustained manner for up to 7 days. Moreover, the initial biological experiments demonstrated high cell viability from the oxygen-generating microparticles and their positive impact on the cell survival, due to their oxygen supply function. Since having optimal oxygen supply is highly vital for cells and tissue to repair and regenerate, we believe that this technology could serve as an important strategy within the field.

Acknowledgments

This work was supported by the Serrapilheira Institute (A.O.L., Serra-1709-19479) and National Council for Scientific and Technological Development (CNPq, #303752/2017-3 and #404683/2018-5 to A.O.L.; and #304133/2017-5 and #424163/2016-0 to F.R.M.) . S. A. gratefully acknowledges financial support from the Sweden-America Foundation (The family Mix Entrepreneur foundation) and the Olle Engkvist Byggmästare Foundation.

Disclosure

The authors declare that they have no conflicts of interest in this work.

References

1. Rai V, Dilisio MF, Dietz NE, Agrawal DK. Recent strategies in cartilage repair: a systemic review of the scaffold development and tissue engineering. *J Biomed Mater Res Part A*. 2017;105:2343–2354. doi:10.1002/jbm.a.36087
2. Lin Z, Willers C, Xu J, Zheng M-H. The chondrocyte: biology and clinical application. *Tissue Eng*. 2006;12:1971–1984. doi:10.1089/ten.2006.12.1971
3. Malda J, Martens DE, Tramper J, Blitterswijk CA, Riesle J. Cartilage tissue engineering: controversy in the effect of oxygen. *Crit Rev Biotechnol*. 2003;23:175–194. doi:10.1080/bty.23.3.175
4. Touri M, Moztarzadeh F, Osman NAA, Dehghan MM, Mozafari M. 3D–printed biphasic calcium phosphate scaffolds coated with an oxygen generating system for enhancing engineered tissue survival. *Mater Sci Eng C*. 2018;84:236–242. doi:10.1016/j.msec.2017.11.037
5. Henrotin Y, Kurz B, Aigner T. Oxygen and reactive oxygen species in cartilage degradation: friends or foes? *Osteoarthritis Cartilage*. 2005;13:643–654. doi:10.1016/j.joca.2005.04.002
6. Gholipourmalekabadi M, Zhao S, Harrison BS, Mozafari M, Seifalian AM. Oxygen-generating biomaterials: a new, viable paradigm for tissue engineering? *Trends Biotechnol*. 2016;34:1010–1021. doi:10.1016/j.tibtech.2016.05.012
7. Yang C, Xiao H, Sun Y, et al. Lipid microbubbles as ultrasound-stimulated oxygen carriers for controllable oxygen release for tumor reoxygenation. *Ultrasound Med Biol*. 2018;44(2):416–425. doi:10.1016/j.ultrasmedbio.2017.08.1883
8. Maio A, Scaffaro R, Lentini L, Piccionello AP, Pibiri I. Perfluorocarbons–graphene oxide nanoplatforms as biocompatible oxygen reservoirs. *Chem Eng J*. 2018;334:54–65. doi:10.1016/j.cej.2017.10.032
9. Ma T, Zhu L, Yang Y, et al. Enhanced in vivo survival of Schwann cells by a synthetic oxygen carrier promotes sciatic nerve regeneration and functional recovery. *J Tissue Eng Regener Med*. 2018;12:e177–e189. doi:10.1002/term.2284
10. Solorio LD, Vieregge EL, Dhami CD, Alsberg E. High-density cell systems incorporating polymer microspheres as microenvironmental regulators in engineered cartilage tissues. *Tissue Eng Part B Rev*. 2013;19:209–220. doi:10.1089/ten.teb.2012.0252
11. Kowalski PS, Bhattacharya C, Afewerki S, Langer R. Smart biomaterials: recent advances and future directions. *ACS Biomater Sci Eng*. 2018;4:3809–3817. doi:10.1021/acsbiomaterials.8b00889
12. Farris AL, Rindone AN, Grayson WL. Oxygen delivering biomaterials for tissue engineering. *J Mater Chem B*. 2016;4:3422–3432. doi:10.1039/C5TB02635K
13. Saveleva MS, Ivanov AN, Kurtukova MO, et al. Hybrid PCL/CaCO3 scaffolds with capabilities of carrying biologically active molecules: synthesis, loading and in vivo applications. *Mater Sci Eng C*. 2018;85:57–67. doi:10.1016/j.msec.2017.12.019
14. Harrison BS, Eberli D, Lee SJ, Atala A, Yoo JJ. Oxygen producing biomaterials for tissue regeneration. *Biomaterials*. 2007;28:4628–4634. doi:10.1016/j.biomaterials.2007.07.003
15. Ward CL, Corona BT, Yoo JJ, Harrison BS, Christ GJ. Oxygen generating biomaterials preserve skeletal muscle homeostasis under hypoxic and ischemic conditions. *PLoS One*. 2013;8:e72485. doi:10.1371/journal.pone.0072485
16. Camci-Unal G, Alemdar N, Annabi N, Khademhosseini A. Oxygen releasing biomaterials for tissue engineering. *Polym Int*. 2013;62:843–848. doi:10.1002/pi.4502
17. Li Z, Guo X, Guan J. An oxygen release system to augment cardiac progenitor cell survival and differentiation under hypoxic condition. *Biomaterials*. 2012;33:5914–5923. doi:10.1016/j.biomaterials.2012.05.012
18. Abdi SIH, Choi JY, Lau HC, Lim JO. Controlled release of oxygen from PLGA-alginate layered matrix and its in vitro characterization on the viability of muscle cells under hypoxic environment. *Tissue Eng Regener Med*. 2013;10:131–138. doi:10.1007/s13770-013-0391-7
19. Benz S, Nötzli S, Siegel JS, Eberli D, Jessen HJ. Controlled oxygen release from pyridone endoperoxides promotes cell survival under anoxic conditions. *J Med Chem*. 2013;56:10171–10182. doi:10.1021/jm4016137
20. Huang -C-C, Chia W-T, Chung M-F, et al. An implantable depot that can generate oxygen in situ for overcoming hypoxia-induced resistance to anticancer drugs in chemotherapy. *J Am Chem Soc*. 2016;138:5222–5225. doi:10.1021/jacs.6b01784

21. Lee H-Y, Kim H-W, Lee JH, Oh SH. Controlling oxygen release from hollow microparticles for prolonged cell survival under hypoxic environment. *Biomaterials*. 2015;53:583–591. doi:10.1016/j.biomaterials.2015.02.117
22. McReynolds J, Wen Y, Li X, Guan J, Jin S. Modeling spatial distribution of oxygen in 3d culture of islet beta-cells. *Biotechnol Pro*. 2017;33:221–228. doi:10.1002/btpr.2395
23. Mora-Huertas CE, Fessi H, Elaissari A. Polymer-based nanocapsules for drug delivery. *Int J Pharm*. 2010;385:113–142. doi:10.1016/j.ijpharm.2009.10.018
24. Li W, Zhang L, Ge X, et al. Microfluidic fabrication of microparticles for biomedical applications. *Chem Soc Rev*. 2018;47:5646–5683. doi:10.1039/C7CS00263G
25. Yeo LY, Gagnon Z, Chang H-C. AC electrospray biomaterials synthesis. *Biomaterials*. 2005;26:6122–6128. doi:10.1016/j.biomaterials.2005.03.033
26. Wang H, Liu Q, Yang Q, et al. Electrospun poly(methyl methacrylate) nanofibers and microparticles. *J Mater Sci*. 2010;45:1032–1038. doi:10.1007/s10853-009-4035-1
27. Nath SD, Son S, Sadiasa A, Min YK, Lee BT. Preparation and characterization of PLGA microspheres by the electrospraying method for delivering simvastatin for bone regeneration. *Int J Pharm*. 2013;443:87–94. doi:10.1016/j.ijpharm.2012.12.037
28. Correia DM, Gonçalves R, Ribeiro C, et al. Electrosprayed poly (vinylidene fluoride) microparticles for tissue engineering applications. *RSC Adv*. 2014;4:33013–33021. doi:10.1039/C4RA04581E
29. Heydari Z, Mohebbi-Kalhori D, Afarani MS. Engineered electrospun polycaprolactone (PCL)/octacalcium phosphate (OCP) scaffold for bone tissue engineering. *Mater Sci Eng C*. 2017;81:127–132. doi:10.1016/j.msec.2017.07.041
30. Kim MK, Lee JY, Oh H, et al. Effect of shear viscosity on the preparation of sphere-like silk fibroin microparticles by electrospraying. *Int J Biol Macromol*. 2015;79:988–995. doi:10.1016/j.ijbiomac.2015.05.040
31. Lee JH, Woo DK, Kim TH, et al. In vitro and long-term (2-year follow-up) in vivo osteogenic activities of human periosteum-derived osteoblasts seeded into growth factor-releasing polycaprolactone/pluronic F127 beads scaffolds. *J Biomed Mater Res Part A*. 2017;105:363–376. doi:10.1002/jbm.a.35907
32. Kwon SK, Song JJ, Cho CG, et al. Tracheal reconstruction with asymmetrically porous polycaprolactone/pluronic F127 membranes. *Head Neck*. 2014;36:643–651. doi:10.1002/hed.23343
33. Wu B, Wu Y, Lu WF, Fuh JY. Polycaprolactone/Pluronic F127 tissue engineering scaffolds via electrohydrodynamic jetting for gastro intestinal repair. *Procedia Cirp*. 2017;65:184–188. doi:10.1016/j.procir.2017.04.045
34. Faramarzi A-R, Barzin J, Mobedi H. Effect of solution and apparatus parameters on the morphology and size of electrosprayed PLGA microparticles. *Fibers Polym*. 2016;17:1806–1819. doi:10.1007/s12221-016-6685-3
35. Dhanka M, Shetty C, Srivastava R. Injectable methotrexate loaded polycaprolactone microspheres: physicochemical characterization, biocompatibility, and hemocompatibility evaluation. *Mater Sci Eng C*. 2017;81:542–550. doi:10.1016/j.msec.2017.08.055
36. Madan SS, Wasewar KL, Ravi Kumar C. Adsorption kinetics, thermodynamics, and equilibrium of α-toluic acid onto calcium peroxide nanoparticles. *Adv Powder Technol*. 2016;27:2112–2120. doi:10.1016/j.apt.2016.07.024
37. Yeh C-S, Wang R, Chang W-C, Shih Y-H. Synthesis and characterization of stabilized oxygen- releasing CaO2 nanoparticles for bioremediation. *J Environ Manage*. 2018;212:17–22. doi:10.1016/j.jenvman.2018.01.068
38. Khodaveisi J, Banejad H, Afkhami A, Olyaie E, Lashgari S, Dashti R. Synthesis of calcium peroxide nanoparticles as an innovative reagent for in situ chemical oxidation. *J Hazard Mater*. 2011;192:1437–1440. doi:10.1016/j.jhazmat.2011.06.060
39. Rastinfard A, Nazarpak MH, Moztarzadeh F. Controlled chemical synthesis of CaO2 particles coated with polyethylene glycol: characterization of crystallite size and oxygen release kinetics. *RSC Adv*. 2018;8:91–101. doi:10.1039/C7RA08758F
40. Elzubair A, Elias CN, Suarez JCM, Lopes HP, Vieira MVB. The physical characterization of a thermoplastic polymer for endodontic obturation. *J Dent*. 2006;34:784–789. doi:10.1016/j.jdent.2006.03.002
41. Abdelrazek EM, Hezma AM, El-khodary A, Elzayat AM. Spectroscopic studies and thermal properties of PCL/PMMA biopolymer blend. *EJBAS*. 2016;3:10–15. doi:10.1016/j.ejbas.2015.06.001
42. Yusoh K, Kumaran SV, Ismail FS. Surface modification of nanoclay for the synthesis of polycaprolactone (PCL) – clay nanocomposite. *MATEC Web of Conf*. 2018;150:02005. doi:10.1051/matecconf/201815002005
43. Ranjbarvan P, Soleimani M, Samadi Kuchaksaraei A, Ai J, Faridi Majidi R, Verdi J. Skin regeneration stimulation: the role of PCL-platelet gel nanofibrous scaffold. *Microsc Res Techn*. 2017;80:495–503. doi:10.1002/jemt.22821
44. Ramyadevi D, Sandhya P. Dual sustained release delivery system for multiple route therapy of an antiviral drug. *Drug Deliv*. 2014;21:276–292. doi:10.3109/10717544.2013.839368
45. Gladysheva TV, Gladyshev NF, Solomonenko EV, Dvoretskii SI. Nanocrystalline calcium peroxide: synthesis, thermal and chemosorption properties. *Russ J Inorg Chem*. 2016;61:1070–1073. doi:10.1134/S0036023616090059
46. Khandanlou R, Ahmad MB, Shameli K, Saki E, Kalantari K. Studies on properties of rice straw/polymer nanocomposites based on polycaprolactone and Fe3O4 nanoparticles and evaluation of antibacterial activity. *Int J Mol Sci*. 2014;15:18466–18483. doi:10.3390/ijms151018466
47. Ray SS, Bousmina M. Biodegradable polymers and their layered silicate nanocomposites: in greening the 21st century materials world. *Prog Mater Sci*. 2005;50:962–1079. doi:10.1016/j.pmatsci.2005.05.002
48. Madan SS, W A U, Wasewar KL. Adsorption of α-toluic acid by calcium peroxide nanoparticles. *Desalin Water Treat*. 2016;57:16507–16513. doi:10.1080/19443994.2015.1079255
49. Massalimov IA, Shayakhmetov AU, Mustafin AG. Specific features of thermal decomposition of mechanically activated calcium peroxide. *Russ J Appl Chem*. 2010;83:1794–1798. doi:10.1134/S1070427210100113
50. Monteiro M, Tavares MIB. The development and characterization of polycaprolactone and titanium dioxide hybrids. *Adv Nanopart*. 2018;7:11–27. doi:10.4236/anp.2018.71002
51. Kumar A, Sawant K. Encapsulation of exemestane in polycaprolactone nanoparticles: optimization, characterization, and release kinetics. *Cancer Nanotechnol*. 2013;4:57–71. doi:10.1007/s12645-013-0037-4
52. Zelenková T, Mora MJ, Barresi AA, Granero GE, Fissore D. On the production of chitosan- coated polycaprolactone nanoparticles in a confined impinging jet reactor. *J Pharm Sci*. 2018;107:1157–1166. doi:10.1016/j.xphs.2017.11.020
53. Kim TH, Oh SH, Na SY, Chun SY, Lee JH. Effect of biological/physical stimulation on guided bone regeneration through asymmetrically porous membrane. *J Biomed Mater Res Part A*. 2012;100:1512–1520. doi:10.1002/jbm.a.34086
54. Lee JI, Yoo HS. Biodegradable microspheres containing poly(ε-caprolactone)–Pluronic block copolymers for temperature-responsive release of proteins. *Colloids Surf B*. 2008;61:81–87. doi:10.1016/j.colsurfb.2007.07.008
55. Oh SH, Kim TH, Chun SY, Park EK, Lee JH. Enhanced guided bone regeneration by asymmetrically porous PCL/pluronic F127 membrane and ultrasound stimulation. *J Biomater Sci Polym*. 2012;23:1673–1686. doi:10.1163/092050611X589518
56. Wang J-C, Liu W, Tu Q, et al. High throughput and multiplex localization of proteins and cells for in situ micropatterning using pneumatic microfluidics. *Analyst*. 2015;140:827–836. doi:10.1039/C4AN01972E

57. Fermor B, Christensen SE, Youn I, Cernanec JM, Davies CM, Weinberg JB. Oxygen, nitric oxide and articular cartilage. *Eur Cell Mater*. 2007;13:56–65. doi:10.22203/ecm.v013a06
58. Rajpurohit R, Koch CJ, Tao Z, Teixeira CM, Shapiro IM. Adaptation of chondrocytes to low oxygen tension: relationship between hypoxia and cellular metabolism. *J Cell Physiol*. 1996;168:424–432. doi:10.1002/(SICI)1097-4652(199608)168:2≤424::AID-JCP21≥3.0.CO;2-1
59. Grimshaw MJ, Mason RM. Bovine articular chondrocyte function in vitro depends upon oxygen tension. *Osteoarthritis Cartilage*. 2000;8:386–392. doi:10.1053/joca.1999.0314
60. Oh SH, Ward CL, Atala A, Yoo JJ, Harrison BS. Oxygen generating scaffolds for enhancing engineered tissue survival. *Biomaterials*. 2009;30:757–762. doi:10.1016/j.biomaterials.2008.09.065
61. Fan Z, Xu Z, Niu H, et al. An injectable oxygen release system to augment cell survival and promote cardiac repair following myocardial infarction. *Sci Rep*. 2018;8:1371. doi:10.1038/s41598-018-19906-w
62. Abdi SI, Ng SM, Lim JO. An enzyme-modulated oxygen-producing micro-system for regenerative therapeutics. *Int J Pharm*. 2011;409:203–205. doi:10.1016/j.ijpharm.2011.02.041
63. Huang Y-C, Leung VY, Lu WW, Luk KD. The effects of microenvironment in mesenchymal stem cell–based regeneration of intervertebral disc. *Spine J*. 2013;13:352–362. doi:10.1016/j.spinee.2012.12.005
64. Lv X, Li Z, Chen S, et al. Structural and functional evaluation of oxygenating keratin/silk fibroin scaffold and initial assessment of their potential for urethral tissue engineering. *Biomaterials*. 2016;84:99–110. doi:10.1016/j.biomaterials.2016.01.032
65. Shiekh PA, Singh A, Kumar A. Oxygen-releasing antioxidant cryogel scaffolds with sustained oxygen delivery for tissue engineering applications. *ACS Appl Mater Interfaces*. 2018;10:18458–18469. doi:10.1021/acsami.8b01736
66. Müller AS, Janjić K, Lilaj B, Edelmayer M, Agis H. Hypoxia-based strategies for regenerative dentistry – views from the different dental fields. *Arch Oral Biol*. 2017;81:121–130. doi:10.1016/j.archoralbio.2017.04.029
67. Loeffler J, Duda GN, Sass FA, Dienelt A. The metabolic microenvironment steers bone tissue regeneration. *Trends Endocrinol Metab*. 2018;29:99–110. doi:10.1016/j.tem.2017.11.008
68. Bonventre JV, Weinberg JM. Recent advances in the pathophysiology of ischemic acute renal failure. *J Am Soc Nephrol*. 2003;14:2199–2210. doi:10.1097/01.ASN.0000079785.13922.F6
69. Zhang M, Kiratiwongwan T, Shen W. Oxygen-releasing polycaprolactone/calcium peroxide composite microspheres. *J Biomed Mater Res*. 2019;1–10. doi:10.1002/jbm.b.34461
70. Budhwani KI, Dettmann MA, Saleh MN, Thomas V. Nano and microbubble systems for on- demand cancer drug delivery. *Curr Nanosci*. 2018;14:33–41. doi:10.2174/1573413713666171009160858
71. Yaghoobi N, Majidi RF, Ali Faramarzi M, Baharifar H, Amani A. Preparation, optimization and activity evaluation of PLGA/streptokinase nanoparticles using electrospray. *Adv Pharm Bull*. 2017;7:131–139. doi:10.15171/apb.2017.017